physica status solidi

pss

www.pss-journals.com

reprint

WILEY-VCH

Wiley Online Library
Early View publication on www.wileyonlinelibrary.com
(issue and page numbers not yet assigned;
citable using Digital Object Identifier – **DOI**)

Phys. Status Solidi B, 1–8 (2016) / **DOI** 10.1002/pssb.201552735

physica status solidi b
www.pss-b.com
basic solid state physics

Reduction of exciton mass by uniaxial stress in GaAs/AlGaAs quantum wells

D. K. Loginov[*,1], P. S. Grigoryev[1], Yu. P. Efimov[2], S. A. Eliseev[2], V. A. Lovtcius[2], V. V. Petrov[2], E. V. Ubyivovk[3,4], and I. V. Ignatiev[1]

[1] Spin Optics Laboratory, St. Petersburg State University, 1, Ulianovskaya str., Petrodvorets, St. Petersburg 198504, Russia
[2] Resource Center "Nanophotonics", St. Petersburg State University, 1, Ulianovskaya str., Petrodvorets, St. Petersburg 198504, Russia
[3] ITMO University, 49 Kronverksky Pr., St. Petersburg 197101, Russia
[4] Faculty of Physics, St. Petersburg State University, 1, Ulianovskaya str., Petrodvorets, St. Petersburg 198504, Russia

Received 25 November 2015, revised 19 February 2016, accepted 25 February 2016
Published online 24 March 2016

Keywords excitonic mass, excitons, polaritons, quantum wells, strain

[*] Corresponding author: e-mail loginov999@gmail.com, Phone: +7-812-4284840, Fax: +7-812-4287240

We show experimentally that the uniaxial stress applied along the twofold symmetry axis of a high-quality heterostructure containing a wide GaAs/AlGaAs quantum well leads to considerable modification of the exciton-polariton reflectivity spectra. We observe: (i) the energy splitting of the light-hole and heavy-hole exciton resonances to appear and (ii) the increase of the quasiperiod (divergence) of spectral oscillations related to the optically allowed exciton-polariton transitions. A theoretical analysis shows that the first effect is due to the strain-induced reduction of crystal symmetry. The divergence of spectral oscillations is found to be due to the strain-induced decrease of the heavy-hole exciton mass. The effective mass is reduced by 5% at the pressure of $P = 0.23$ GPa. This effect shows the potentiality of spectroscopic ways of strain detection in semiconductors.

1 Introduction Optical spectroscopy has proven to be an efficient method to study excitons in semiconductor structures. It reveals coupling to light and size quantization of excitons confined in thin semiconductor crystals or wide quantum wells (QW) [1, 2]. The QW interfaces break the wave vector selection rules for optical transitions. In particular, this concerns the transitions from or to exciton states with large wave vectors, $K > q$, where q is the wave vector of light at the exciton resonance frequency. This symmetry lowering leads to the appearance of quasiperiodic spectral oscillations in reflectivity spectra [3, 4]. Multiple experimental studies show that these oscillations manifest quantization of the center-of-mass exciton motion [2, 5–14]. By introducing an effective wave vector for each quantum-confined state, one can extract the exciton energy dispersion, that is the dependence of the exciton kinetic energy on its wave vector, **K**, from the observed spectral features.

An efficient approach to the analysis of the exciton optical response is the polaritonic model, which accounts for the modification of exciton dispersion due to its coupling to light, thus allowing one to model the reflectivity spectra [10, 15–19]. Previous studies have clearly shown that the dispersion is weakly affected by the QW confinement for the well width of $L_{QW} > 6a_B$, where a_B is the exciton Bohr radius [6]. This is why the bulk exciton dispersion can be studied experimentally in wide QWs. The spectral positions of exciton (exciton-polariton) resonances in these structures are dependent on the exciton effective mass [20].

In GaAs-type crystals with degenerated valence band, the effective masses of heavy-hole and light-hole excitons are most thoroughly studied [15, 16]. The exciton mass is very sensitive to various types of interactions that may induce heavy-hole–light-hole mixing (hh–lh mixing). In particular, the heavy-hole and light-hole subbands are coupled by the electron–hole Coulomb interaction and by the QW potential [21–23]. As is shown in these papers, this coupling results in several effects, in particular, in a nonparabolicity of exciton dispersion and in a change of exciton mass. The hh–lh coupling and, consequently, the exciton dispersion can be also modified by external perturbations, e.g., by the external magnetic field applied along the exciton confinement direction (Faraday geometry) [11–14]. The authors of these papers observed a magnetic-field-induced change of exciton dispersion, which was treated as the result of exciton states mixing. They discussed the observed effects in terms of a change of exciton mass.

Mechanical strain causing the splitting of the valence band changes the hh–lh coupling strength and may strongly affect the exciton dispersion. The strain can be induced by internal forces in heterostructures with the lattice-mismatched layers, e.g., InGaAs/GaAs structures [24–27]. An application of external stress is an efficient method of control of the hh–lh coupling and its effect on the exciton spectra [28–32].

The strain causes energy shifts of exciton states due to a change of the bandgap. The experimental study of these energy shifts in optical experiments allows one to determine deformation potentials. The knowledge of deformation potentials is of practical importance, e.g., for the fabrication of semiconductor devices consisting of layers with different lattice constants.

Many experimental works have been devoted to the strain-induced effects in heterostructures with relatively narrow QWs, $L \leq 30$ nm, and superlattices as well as in QW-based devices, see, e.g., Refs. [33–40]. The authors demonstrate the efficiency of the application of external stress to the control of the hh–lh coupling and, correspondingly, of various properties of such devices as laser diodes and high-electron-mobility transistors (HEMPTs). Introduction of a local pressure by a pin has been also used to create a trap for polaritons in a microcavity [41, 42].

The basic theory of strain-induced effects in semiconductors was developed by Bir and Pikus [28]. It is applied in the works we cited above for the analysis of the strain-induced shift of exciton states in narrow QWs. No experimental evidence for the effect of uniaxial strain on the polariton states in wide QWs has been reported so far, to the best of our knowledge. A theoretical analysis of the strain effect in a wide GaAs QW is given in Ref. [43], where a uniaxial stress applied along the crystal axis [100] is considered. A remarkable change (convergence) of masses of the heavy- and light-hole excitons has been predicted in this work.

The present work is devoted to the theoretical and experimental studies of the mass-convergence effect in polariton reflectivity spectra of a wide QW in the presence of a uniaxial stress applied along the [110] axis. The application of stress in this direction is of practical importance because chipping the structure perpendicular to [110] allows one to easily obtain a piece of the structure with strongly parallel planes. This property of the GaAs-based structures is frequently exploited, for example, for preparation of semiconductor lasers [38]. We used this property to prepare a sample for our experiments. The high quality of the structure studied has allowed us to observe many spectral oscillations, which are shifted to the higher energy if pressure is applied. Remarkably, the shift increases with the increase of the quantum number N of the confined exciton state, and it reaches 5 meV for $N = 16$ at the pressure of $P = 0.23$ GPa. We have modeled theoretically the strain effect on the exciton dispersion using the method similar to one described in Ref. [43] for the strain applied along the [100] axis.

2 Exciton Hamiltonian in a crystal under uniaxial stress We consider an exciton propagating along the z-axis (crystal axis [001]) in a crystal characterized by the zinc-blende symmetry. We restrict our discussion of the excitons with wave vectors $|\mathbf{K}| > 1/a_\mathrm{B}$ corresponding to the "large-exciton-momentum limit" [23]. The experimentally observed spectral oscillations (see Section 4) well correspond to this limit of wave vectors. We therefore ignore several less important effects, such as the exchange coupling of exciton states, the nonparabolicity of exciton dispersion, and the coupling of the ground and excited exciton states, extensively discussed in the narrow QW limit $|\mathbf{K}| < 1/a_\mathrm{B}$ [44]. We also neglect the effects related to the corrugation of the valence band [23]. They are weak and do not directly affect spectral resonances in our system.

In the framework of the approximations introduced, the exciton energy in a crystal with no strain is as follows [23]:

$$H^{(0)}_{\mathrm{Xh,l}} = E_\mathrm{g} - R_\mathrm{X} + \frac{\hbar^2 K_z^2}{2M_\mathrm{h,l}}. \tag{1}$$

Here, E_g is the band gap and R_X is the exciton binding energy, K_z is z-component of the exciton center-of-mass wave vector. The translational masses of the heavy-hole and light-hole excitons are defined as: $M_\mathrm{h,l} = m_\mathrm{e} + m_\mathrm{h,l}$, with effective masses of electron, m_e, and hole, $m_\mathrm{h,l} = m_0/(\gamma_1 \mp 2\gamma_2)$. Here, γ_1 and γ_2 are the Luttinger parameters and m_0 is the free electron mass.

The Hamiltonian of an exciton, according to Ref. [23], is represented by an 8×8 matrix consisting of two identical diagonal 4×4 blocks. The first block describes the optically active heavy-hole and light-hole exciton states (exciton spin projections $J_z = \pm 1$), whereas the second one represents the optically inactive states ($J_z = 0, \pm 2$).

Basic wave functions of such a Hamiltonian include the wave function of a moving exciton, $\Psi(K_z)$, as the coordinate part and the eight-component spinor with one nonzero component, $v_{j,s}$:

$$|j, s\rangle = v_{j,s}\Psi(K_z), \tag{2}$$

where $j = \pm 3/2, \ \pm 1/2$, and $s = \pm 1/2$ are the projections of the spin moments of the hole and the electron, respectively, to the z-axis.

Let us now consider the impact of uniaxial strain P applied along the [110] axis. Components of the strain tensor have a simple form [28, 45]:

$$\begin{aligned}
\varepsilon_{xx} &= \varepsilon_{yy} = -(S_{11} + S_{12})\frac{1}{2}P, \\
\varepsilon_{zz} &= -S_{12}P, \\
\varepsilon_{xy} &= -S_{44}\frac{1}{2}P, \\
\varepsilon_{xz} &= \varepsilon_{yz} = 0,
\end{aligned} \tag{3}$$

where S_{11}, S_{12}, and S_{44} are components of the elastic compliance tensor. Such strain, in particular, leads to the appearance of the linear in the hole wave-vector terms in the Hamiltonian [46, 47]. In the case under consideration, these terms

couple the exciton 1s- and np-states and lead to variation of the exciton binding energy. However, this change is small comparing to the effects discussed in the present paper.

The most remarkable effect of the crystal strain is the alteration of the valence band Γ_8 described by the Bir–Pikus Hamiltonian [28, 46]. This Hamiltonian does not couple the optically active and inactive states. Therefore, we consider only the 4×4 block with basic functions $|j, s\rangle = |\pm 3/2, \mp 1/2\rangle,\ |\pm 1/2, \pm 1/2\rangle$ describing the optically active states.

To simplify our analysis, we change the basis (2) as follows:

$$|h\alpha\rangle = \frac{1}{\sqrt{2}}|3/2, -1/2\rangle \pm \frac{i}{\sqrt{2}}|-3/2, 1/2\rangle,$$
$$|l\alpha\rangle = \frac{1}{\sqrt{2}}|1/2, 1/2\rangle \pm \frac{i}{\sqrt{2}}|-1/2, -1/2\rangle. \quad (4)$$

Here, the upper and lower signs correspond to the indices $\alpha = x'$ and $\alpha = y'$, respectively. These states can be excited by the light polarized along [110] and [1$\bar{1}$0] axes, which are the axes of optical anisotropy induced by the uniaxial strain.

A matrix of the exciton Hamiltonian for optically active states constructed using wave functions (4) is composed of two 2×2 blocks:

$$\hat{H}_X = \begin{pmatrix} H_{h\alpha} & V \\ V^* & H_{l\alpha} \end{pmatrix}, \quad \text{where } \alpha = x',\ y'. \quad (5)$$

Here,

$$H_{hx'} = H_{hy'} = H_{Xh}^{(0)} - \left(a - \frac{b}{2}\right)(S_{11} + S_{12})\,P,$$
$$H_{lx'} = H_{ly'} = H_{Xl}^{(0)} - \left(a + \frac{b}{2}\right)(S_{11} + S_{12})\,P,$$
$$V = i\frac{d}{4}S_{44}P, \quad (6)$$

where a, b, and d are the deformation potentials [28]. Since the states corresponding to $\alpha = x'$ and $\alpha = y'$ are decoupled, the problem for each such block can be solved independently.

The solution of the eigenvalue problem for the Hamiltonian (5) is trivial:

$$E_{1,2} = \frac{1}{2}\left(H_{h\alpha} + H_{l\alpha} \pm \sqrt{(H_{h\alpha} - H_{l\alpha})^2 + 4|V|^2}\right). \quad (7)$$

This shows that the deformation potential a is accounted for in the sum of terms: $H_{h\alpha} + H_{l\alpha}$, that governs the overall shift of the quantum-confined exciton states. Deformation potentials b and d are included in the expression under the square root and, therefore, they govern the splitting of the heavy-hole and light-hole exciton bands. This splitting depends also on the exciton wave vector K so that the applied strain modifies the exciton dispersion. This dependence is important for the interpretation of the polariton spectra in Section 4. Here, we would like to note that perturbation V plays a similar role as an operator that splits the conduction and valence bands in topological insulators, superconductors, and graphene, which results in the appearance of a nonzero mass [48–50].

The uniaxial strain also couples the light-hole states with the split-off valence-band states, alterating the light-hole mass [28]. Estimates show that the energy shifts of the exciton states caused by this coupling are small compared to those caused by the hh–lh coupling. This is why we do not consider this effect in what follows.

The theoretical model considered above allows one to also analyze the tensile strain. In particular, as it follows from Eqs. (6) and (7) for case $P < 0$, the ground state of the light-hole exciton is shifted lower in energy than that of the heavy-hole exciton. Because the dispersion curvature for the light-hole exciton is larger than that for heavy-hole exciton, they are crossed at some wave vector K. Mixing of the heavy-hole and light-hole exciton states results in the anticrossing of these dispersion curves that strongly modify the exciton dispersion. We will not discuss the tensile strain in detail because our experimental data are obtained only for positive stress.

3 Dielectric permittivity in the presence of uniaxial strain In our analysis of the reflectivity spectra, we employ a model of the polariton wave interference in a wide QW described, e.g., in Refs. [2, 16, 19, 10]. We assume that the incident light is directed perpendicular to the sample surface and linearly polarized along one of the optical anisotropy axes. The exciton–photon interaction is described by the perturbation operator (see, e.g., Ref. [51]):

$$V_d = -(d_h + d_l)E^{(\alpha)},\ (\alpha = x',\ y'), \quad (8)$$

where $E^{(\alpha)}$ is the electric field of a light wave and $d_{h,l}$ are the dipole matrix elements for heavy-hole and light-hole excitons. The square of the matrix elements can be expressed as: $d_h^2 = 3d_l^2 = \hbar\omega_{LT}\epsilon_0\Omega$, where $\hbar\omega_{LT}$ is the energy of the longitudinal–transverse splitting [15], ϵ_0 is the background permittivity, and Ω is the crystal volume [52].

The excitonic component of the polariton wave function is a linear combination of heavy- and light-hole exciton wave functions (4):

$$\Psi_\alpha(K_z) = C_{vac}|vac\rangle + \sum_{\beta=h,l} C_{\beta\alpha}|\beta\alpha\rangle, \quad (9)$$

where $C_{\beta\alpha}$, C_{vac} are the expansion coefficients and $|vac\rangle$ is the crystal vacuum state.

Dispersion relations, wave functions, and permittivity with respect to exciton–photon interactions can be obtained following the method described, e.g., in Refs. [43, 51]. To this end, one should first solve a secular equation taking into

account interactions (8):

$$\begin{pmatrix} H_{h\alpha}-\hbar\omega & V & -d_h E^{(\alpha)} \\ V^* & H_{l\alpha}-\hbar\omega & -d_l E^{(\alpha)} \\ -d_h E^{(\alpha)} & -d_l E^{(\alpha)} & H_{vac}-\hbar\omega \end{pmatrix} \begin{pmatrix} C_{h\alpha} \\ C_{l\alpha} \\ C_{vac} \end{pmatrix} = 0. \tag{10}$$

Here, $H_{vac} = 0$ is the energy of the vacuum state and $\hbar\omega$ is the photon energy. The expansion coefficients $C_{h,l\alpha}$ can be easily found from this matrix equation in the limit of very weak optical excitation where $C_{vac} \approx 1$.

Resonant polarization of the medium due to exciton–photon coupling can be now expressed in terms of the $C_{h,l\alpha}$ coefficients [16, 51]:

$$\begin{aligned} 4\pi\mathcal{P}^{(\alpha)} &= \frac{1}{\Omega}\langle\Psi_\alpha|e\cdot r|\Psi_\alpha\rangle = \frac{1}{\Omega}(d_h C_{h\alpha} + d_l C_{l\alpha}) \\ &= 4\pi\chi_{l\alpha}E^{(\alpha)} + 4\pi\chi_{h\alpha}E^{(\alpha)}. \end{aligned} \tag{11}$$

This expression defines contributions to the optical susceptibility from the heavy-hole and light-hole exciton resonances, $\chi_{h,l\alpha}$. The resonant susceptibility is obtained from Eq. (10):

$$\begin{aligned} 4\pi\chi_{h\alpha} &= \frac{\tilde{H}_{l\alpha}\hbar\omega_{LT}}{\tilde{H}_{h\alpha}\tilde{H}_{l\alpha} - |V|^2} \pm \frac{1}{\sqrt{3}}\frac{V\hbar\omega_{LT}}{\tilde{H}_{l\alpha}\tilde{H}_{h\alpha} - |V|^2}, \\ 4\pi\chi_{l\alpha} &= \frac{1}{3}\frac{\tilde{H}_{h\alpha}\hbar\omega_{LT}}{\tilde{H}_{h\alpha}\tilde{H}_{l\alpha} - |V|^2} \pm \frac{1}{\sqrt{3}}\frac{V\hbar\omega_{LT}}{\tilde{H}_{l\alpha}\tilde{H}_{h\alpha} - |V|^2}. \end{aligned} \tag{12}$$

Here,

$$\tilde{H}_{h,l\alpha} \equiv H_{h,l\alpha} - \hbar\omega + i\Gamma_{h,l},$$

where $\Gamma_{h,l}$ is a phenomenological parameter introduced to describe processes of energy dissipation. The upper and lower signs in relation (12) correspond to the light polarization along the x' and y' axes. We should stress that the susceptibility $\chi_{h,l\alpha}$ depends on the exciton wave vector $\mathbf{K}$ through $H^{(0)}_{h,l\alpha}$, see Eqs. (1) and (6).

One should also keep in mind that, even without the exciton resonances, the uniaxial strain induces the optical anisotropy of crystals due to the piezo-optic effect [53, 54]. This effect leads to an additional background permittivity, which, in the basis of light waves polarized along x' and y' axes, is described as follows [53, 54]:

$$-\delta\epsilon_{x'} = \delta\epsilon_{y'} = \pi_{44}P \equiv \delta\epsilon, \tag{13}$$

where π_{44} is the component of the piezo-optic tensor.

The total permittivity of the medium that accounts for contributions (12) and (13) has the form:

$$\epsilon_\alpha(\omega, K_z) = \epsilon_0 \pm \delta\epsilon + 4\pi\chi_{h\alpha} + 4\pi\chi_{l\alpha}, \ (\alpha = x', \ y'). \tag{14}$$

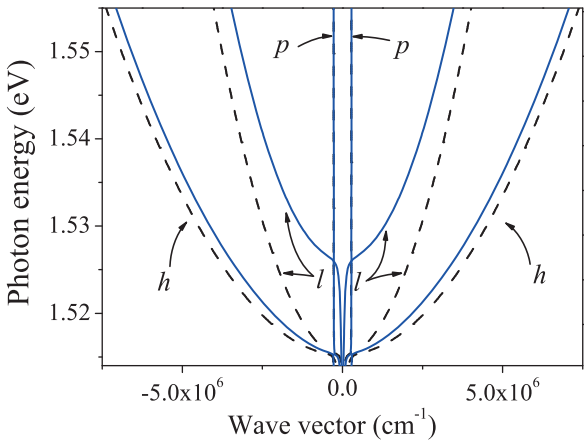

Figure 1 Modification of the dispersion curves for polaritons of h- and l-types in the bulk GaAs under the application of strain along the [110] axis. The black dashed and blue solid curves are the dispersion curves at $P = 0$ and $P = 0.23$ GPa, respectively. The overall shift of the dispersion curves due to the strain is omitted. Notations h, l, and p are explained in the text.

In order to obtain the dispersion relations for polariton eigenmodes, one should solve the dispersion equation [4]:

$$\epsilon_\alpha(\omega, K_z) = \frac{c^2 K_z^2}{\omega^2}, \tag{15}$$

where c is the light velocity and $\epsilon_\alpha(\omega, K_z)$ is described by the expression (14).

Eq. (15) has independent solutions for $\alpha = x'$ and $\alpha = y'$, which correspond to two linear polarizations of the incident light. For each polarization, the equation is a polynomial of the third order over K_z^2. It describes three dispersion branches. An example of the dependences for the strained and unstrained GaAs is shown in Fig. 1. The material parameters used in the calculations are listed in Table 1. Curves in the figure are marked according to the largest expansion coefficient in the polariton wave function at large K_z. Notations "h" and "l" correspond to the heavy-hole and light-hole polariton branches, while "p" stands for the photon-like polariton branch.

The deformation leads to the reduction of the GaAs crystal symmetry group from T_d to D_{2d}. Therefore, the dispersion curves of the exciton-like modes of h- and l-types are shifted to higher energies and are split due to the diagonal terms of Hamiltonian (10). The dispersion curves are additionally split due to the hh–lh coupling described by matrix element V of Hamiltonian (10). As seen in Fig. 1, the h-type branch becomes steeper as the pressure increases. This behavior is a signature of the reduction of effective mass for h-type exciton-polaritons. At the same time, the l-type branch becomes flatter, which is equivalent to the increase of the exciton mass. In the first approximation, this effect can be described as the convergence of effective masses of the h- and l-type exciton-polaritons. We should note that this alteration of polariton mass is different for different directions

Table 1 Material parameters used in computation. Electron mass m_e, bandgap energy E_g, and Luttinger parameters γ_i are taken from Ref. [58]; elastic compliance tensor components S_{ij} are taken from Ref. [59] and given in the 10^{-12} cm^2 dyn^{-1} units; deformation potential constants a, b, and d are taken from Ref. [60].

$\hbar\omega_{LT}$ (meV) [56]	ϵ_0 [57]	m_e (m_0)	γ_1	γ_2	E_g (eV)	S_{11}	S_{12}	S_{44}	π_{44} (GPa^{-1}) [53]	a (eV)	b (eV)	d (eV)
0.08	12.56	0.067	6.8	2.3	1.520	1.172	−0.365	1.68	1.5	−6.7	−1.7	−4.55

of the polariton propagation [28, 55]. In the general case, the uniaxial stress results in an anisotropic change of tensor of the exciton mass. The convergence of the exciton masses is not a universal effect and may occur in some geometries of experiments, in particular, with pressure along the [110] direction for excitons propagating along the [001] direction considered here.

4 Experimental reflectivity spectra and their analysis We have studied a semiconductor structure with the GaAs/$Al_{0.3}Ga_{0.7}As$ quantum well grown by the molecular beam epitaxy on [001] GaAs substrate. The QW width is $L_{QW} = 240$ nm. Besides the QW and barrier layers, the heterostructure contains several thin technological layers GaAs, AlAs, AlGaAs, and a technological superlattice GaAs/AlGaAs of total width 430 nm. All these technological layers are not important for the present study.

The reflectivity spectra have been measured using a standard setup consisting of a white-light source (an incandescent lamp), a 0.5-m monochromator, a helium closed-cycle cryostat, and a photodiode. The lamp radiation filtered by the monochromator was directed at an angle close to normal to the sample surface. Incident light was linearly polarized along the [110] axis. The reflected beam was detected by the photodiode. In the optical scheme used, the photoluminescence of the sample excited by weak monochromatic light was negligibly small and did not affect the detected signal. To apply a stress to the sample, we have designed a mechanical micropress. It consists of two anvils, one of which is fixed and the other one is pressed by a piezotransducer. The sample is fixed between the anvils. An electric voltage is applied to the piezotransducer that results in application of the stress to the sample due to the piezoelectric effect. This method allowed us to apply the stress to the sample under study in the vacuum chamber of the closed-cycle cryostat we used. The micropress with the sample was attached to a cold finger in the cryostat and cooled to a temperature $T = 12$ K. The magnitude of applied stress was obtained from the spectral positions of dominant spectral features for the heavy-hole and light-hole excitons using Eq. (7) for $K_z = 0$ and deformation potentials from Ref. [60].

Examples of measured spectra are shown in Fig. 2a. The dominant feature at the photon energy of about 1.516 eV at zero pressure is related to the interference of polaritonic waves in the range of anti-crossing of exciton-like and photon-like polaritonic modes at $\mathbf{K} = \mathbf{q}$ [15, 16]. In the spectrum of the stressed heterostructure, the dominant feature is split into exciton resonances corresponding to the ground states of the heavy-hole and light-hole excitons.

Besides the dominant features, quasiperiodical oscillations are observed in Fig. 2a. The oscillations are caused by the interference of the photon-like modes and the exciton-like modes with large K-vector [1, 2, 11, 43, 12, 10]. We should note here that the observation of such spectral oscillations is possible only in high-quality QW structures.

To simulate the reflectivity spectra, it is necessary to consider the interference of light waves reflected from the sample surface and three polariton modes propagating in the QW. The amplitudes of these modes can be determined if one considers the Maxwell's boundary conditions as well as the Pekar's additional boundary conditions [16]. The boundary conditions give rise to a system of linear equations with respect to amplitudes of the electric field of light and polaritonic waves in the structure. The solution of this system allows one to obtain the ratio of amplitudes of the incident (E_i) and reflected (E_r) light waves (see, e.g., Refs. [43, 10]). The reflectivity coefficient is the squared modulus of this ratio: $R(\omega) = |E_r/E_i|^2$.

The reflectivity spectra calculated for a QW of the same width as in the experiment are presented in Fig. 2b for several magnitudes of applied pressure. In the calculations, we

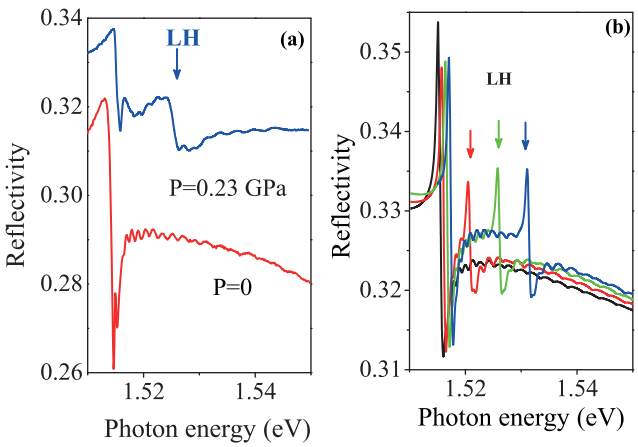

Figure 2 (a) Experimentally measured reflectivity spectra for the GaAs/AlGaAs QW of width $L_{QW} = 240$ nm. Red and blue curves show the spectra measured for pressure $P = 0$ and $P = 0.23$ GPa, respectively. (b) Reflectivity spectra calculated for pressure $P = 0$, 0.1, 0.2, and 0.3 GPa (black, red, green, and blue curves, respectively). The vertical arrows indicate the spectral features related to the split off light-hole exciton (LH).

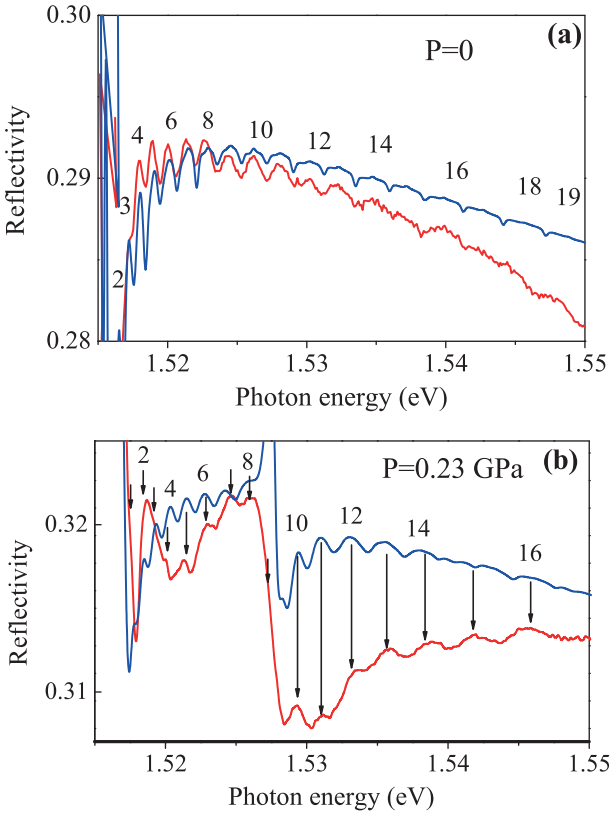

Figure 3 Experimentally measured (red curves) and theoretically calculated (blue curves) reflectivity spectra for the GaAs/AlGaAs QW of width $L_{QW} = 240$ nm for pressures $P = 0$ (a) and $P = 0.23$ GPa (b). Numbers in both panels numerate the oscillations. Vertical arrows in panel (b) indicate respective oscillations in the experimental spectrum.

introduced the near-surface dead layers, $L_D = 19$ nm, for excitons in the QW according to Refs. [61, 62]. The material parameters used are shown in Table 1. For these calculations, we have chosen the damping parameters $\Gamma_h = 0.27$ meV and $\Gamma_l = 0.55$ meV. As seen, the uniaxial stress shifts the light-hole exciton higher in energy than the heavy-hole exciton.

In Fig. 3, the calculated and experimental reflectivity spectra in the energy range above 1.516 eV are compared. We used different damping parameters for strained and unstrained QW to fit the experiment: $\Gamma_h = 0.07$ meV, $\Gamma_l = 0.35$ meV for $P = 0$ and $\Gamma_h = 0.27$ meV, $\Gamma_l = 0.55$ meV for $P = 0.23$ GPa. A possible reason for an increase of the damping parameters with pressure is a strain inhomogeneity. We should note that the damping parameters for the light-hole exciton are larger than those for the heavy-hole one. Such difference is typically observed in experiment (see, Fig. 2a and Ref. [10]).

There is a noticeable difference in general behavior of experimental and of simulated spectra. We attribute this difference to the complex layer structure of our sample, which contains many technological layers. It is well known (see, e.g., Ref. [16]) that the interference of light reflected from several layers may result in slow modulation of a reflectivity spectrum. We ignore technological layers in the simulation for simplicity and focus on the spectral oscillations, containing valuable information on the polariton dispersion. The calculations show that the observed spectral oscillations are mainly caused by the contribution from the h-type modes. The contribution of the l-type modes for $\mathbf{K} \gg \mathbf{q}$ is negligibly small due to its lower oscillator strength and larger inhomogeneous broadening.

The calculated spectra reasonably reproduce the overall behavior of the spectral oscillations observed experimentally (see Fig. 3). In particular, the increase of the energy splitting between the oscillations in the strained QW is reproduced. This is a nontrivial result because deformation potentials b and d describing the oscillation divergence [see Eq. (7)] are obtained from the splitting of valence bands rather than from the study of exciton dispersion [60]. Our results show that the deformation potentials found here are also appropriate for modeling of the strain-induced change of curvature of the dispersion branches.

The quantitative comparison of experimental and simulated spectra is limited by the accuracy of detection of the energy positions of spectral oscillations in our experiments. The accuracy is limited because of the relatively large broadenings of the observed resonances. We note also that only a limited number of the oscillations have been observed. In this sense, further progress in the preparation of high-quality structures is very desirable that would allow one to verify the deformation potentials.

The increase of the oscillation period shown in Fig. 3 manifests the reduction of the effective mass M_h of a heavy-hole exciton. To obtain the exciton mass in a strained QW, we approximate the exciton-like part of the polariton dispersion presented in Fig. 1 by the parabolic function: $E = \hbar^2 K_z^2/(2M_h) + B$. Here, the parameter B describes the edge of the exciton band in the strained structure. An approximation is performed in the range beyond the exciton–light anti-crossing region, $K_z > 1 \times 10^6$ cm^{-1}. The uncertainty of this approximation and, consequently, in the exciton mass extraction is of about 1%.

The obtained exciton mass decrease at $P = 0.23$ GPa is not small: $\Delta M_h = 0.026 m_0$ which is $5 \pm 1.5\%$ of the initial exciton mass. The model described above allows us to estimate variation of the exciton mass at the strongest possible pressure, $P_{max} = 0.8$ GPa, acceptable for GaAs [36, 63]: $\Delta M_h = 0.09\, m_0$ that corresponds to the approximately $14 \pm 2\%$ decrease of the exciton effective mass. The theoretical analysis of Ref. [43] shows that this effect may be even larger when the stress is applied along the [100] crystallographic axis. In particular, the decrease of the heavy-hole exciton mass of about 45% may be obtained at a pressure $P = 0.7$ GPa. It follows from Eqs. (6) and (7) that modification of the exciton dispersion is sensitive to values of the deformation potentials b and d. Therefore, rigorous analysis of the reflectivity spectra of the heterostructures with QWs under uniaxial stress may allow one precise determination of these constants. These material parameters are important from the

fundamental point of view and for practical applications, e.g., for fabrication of laser diodes, HEMTs [38–40], etc.

5 Conclusions We have theoretically and experimentally studied the impact of uniaxial pressure applied along the second-order symmetry axis of a structure with a wide GaAs/AlGaAs QW on the exciton-polariton resonances in the reflectivity spectra. Thanks to the high quality of the interfaces, we could observe in the reflectivity spectra nearly periodical oscillations caused by the interference of photon-like and exciton-like polariton modes in the QW. The uniaxial stress is found to induce the increase of the spectral splitting between oscillations. This effect is understood in terms of the strain-induced coupling of heavy-hole and light-hole exciton states. The coupling results in a modification of the exciton dispersion, which can be treated as the decrease of the effective mass of the heavy-hole exciton. The observation of the exciton mass decrease opens up one more way for the experimental verification of the deformation potential parameters, which are as important for fundamental studies as for practical applications.

Acknowledgements We are grateful to I. Ya. Gerlovin, M. M. Glazov, and A. V. Kavokin for discussions and critical reading of the manuscript. Financial support from the Russian Ministry of Science and Education (contract No. 11.G34.31.0067) and SPbSU (grant No. 11.38.213.2014). P.S.G. acknowledges support from RFBR (grant No. 15-52-12019) in the frame of International Collaborative Research Center TRR 160. I.V.I. thanks RFBR (grant No. 16-02-00245 a) for the financial support. The authors also thank the SPbSU Resource Center "Nanophotonics" (www.photon.spbu.ru) for providing the sample studied in this work.

References

[1] V. A. Kiselev, B. S. Razbirin, and I. N. Uraltsev, Phys. Status Solidi B **72**, 161 (1975).
[2] A. Tredicucci, Y. Chen, F. Bassani, J. Massies, C. Deparis, and G. Neu, Phys. Rev. B **47**, 10348 (1993).
[3] S. I. Pekar, Crystal Optics and Additional Light Waves (Benjamin, New York, 1983)
[4] V. M. Agranovich and V. L. Ginzburg, Crystal Optics with Spatial Dispersion and the Exciton Theory, 2nd edn. (Nauka, Moscow, 1979; Springer, New York, 1984).
[5] Z. K. Tang, A. Yanase, T. Yasui, Y. Segawa, and K. Cho, Phys. Rev. Lett. **71**, 1431 (1993).
[6] N. Tomassini, A. D'Andrea, R. Del Sole, H. Tuffigo-Ulmer, and R. T. Cox, Phys. Rev. B **51**, 5005 (1995).
[7] D. Greco, R. Cingolani, A. D'Andrea, N. Tomassini, L. Vanzetti, and A. Franciosi, Phys. Rev. B **54**, 16998 (1996).
[8] P. Lefebvre, V. Calvo, N. Magnea, T. Taliercio, J. Allégre, and H. Mathieu, Phys. Rev. B **56**, R10040 (1997).
[9] E. V. Ubyivovk, Yu. K. Dolgikh, Yu. P. Efimov, S. A. Eliseev, I. Ya. Gerlovin, I. V. Ignatiev, V. V. Petrov, and V. V. Ovsyankin, J. Lumin. **102–103**, 751 (2003).
[10] D. K. Loginov, E. V. Ubyivovk, Yu. P. Efimov, V. V. Petrov, S. A. Eliseev, Yu. K. Dolgikh, I. V. Ignatiev, V. P. Kochereshko, and A. V. Sel'kin, Fiz. Tverd. Tela **48**, 1979 (2006) [Phys. Solid State **48**, 2100 (2006)].
[11] J. J. Davies, D. Wolverson, V. P. Kochereshko, A. V. Platonov, R. T. Cox, J. Cibert, H. Mariette, C. Bodin, C. Gourgon, E. V. Ubylvovk, Y. P. Efimov, and S. A. Eliseev, Phys. Rev. Lett. **97**, 187403 (2006).
[12] L. C. Smith, J. J. Davies, D. Wolverson, S. Crampin, R. T. Cox, J. Cibert, H. Mariette, V. P. Kochereshko, M. Wiater, G. Karczewski, and T. Wojtowicz, Phys. Rev. B **78**, 085204 (2008).
[13] J. J. Davies, L. C. Smith, D. Wolverson, A. Gust, C. Kruse, D. Hommel, and V. P. Kochereshko, Phys. Rev. B **81**, 085208 (2010).
[14] L. C. Smith, J. J. Davies, D. Wolverson, H. Boukari, H. Mariette, V. P. Kochereshko, and R. T. Phillips, Phys. Rev. B **83**, 155206 (2011).
[15] E. L. Ivchenko, Optical Spectroscopy of Semiconductor Nanotstructures (Alpha Science, Harrow, 2005).
[16] A. V. Kavokin, J. J. Baumberg, G. Malpuech, and F. P. Laussy, Microcavities (Oxford University Press, New York, 2007).
[17] Y. Chen, A. Tredicucci, and F. Bassani, Phys. Rev. B **52**, 1800 (1995).
[18] M. R. Vladimirova, A. V. Kavokin, and M. A. Kaliteevski, Phys. Rev. B **54**, 14566 (1996).
[19] S. A. Markov, R. P. Seisyan, and V. A. Kosobukin, Fiz. Tekh. Poluprovodn. **38**, 230 (2004) [Semiconductors **38**, 225 (2004)].
[20] R. Knox, Theory of Excitons (Academic Press, New York and London, 1963).
[21] M. Altarelli and N. O. Lipari, Phys. Rev. B **15**, 4898 (1977).
[22] M. Altarelli and N. O. Lipari, Phys. Rev. B **15**, 4883 (1977).
[23] E. O. Kane Phys. Rev. B **11**, 3850 (1975).
[24] C. G. Van de Walle, Phys. Rev. B **39**, 1871 (1989).
[25] J.-Y. Marzin, M. N. Charasse, and B. Sermage, Phys. Rev. B **31**, 8298(R) (1985).
[26] Z. S. Piao, M. Nakayama, and H. Nishimura, Phys. Rev. B **54**, 10312 (1996).
[27] A. V. Trifonov, S. N. Korotan, A. S. Kurdyubov, I. Ya. Gerlovin, I. V. Ignatiev, Yu. P. Efimov, S. A. Eliseev, V. V. Petrov, Yu. K. Dolgikh, V. V. Ovsyankin, and A. V. Kavokin, Phys. Rev. B **91**, 115307 (2015).
[28] G. L. Bir and G. E. Pikus, Symmetry and Strain Induced Effects in Semiconductors (Wiley, New York, 1972).
[29] A. Blacha, S. Ves, and M. Cardona, Phys. Rev. B **27**, 6346 (1983).
[30] M. R. Wagner, G. Callsen, J. S. Reparaz, R. Kirste, A. Hoffmann, A. V. Rodina, A. Schleife, F. Bechstedt, and M. R. Phillips, Phys. Rev. B **88**, 235210 (2013).
[31] R. Ishii, A. Kaneta, M. Funato, Y. Kawakami, and A. A. Yamaguchi, Phys. Rev. B **81**, 155202 (2010).
[32] R. Ishii, A. Kaneta, M. Funato, and Y. Kawakami, Phys. Rev. B **87**, 235201 (2013).
[33] J. Lee, C. Jagannath, M. O. Vassell, and E. S. Koteles, Phys. Rev. B **35**, 4164 (1988).
[34] G. Arnaud, J. Allegre, P. Lefebvre, H. Mathieu, L. K. Howard, and D. J. Dunstan, Phys. Rev. B **46**, 15290 (1992).
[35] G. Rau, P. C. Klipstein, V. Nikos Nicopoulos, and N. F. Johnson, Phys. Rev. B **54**, 5700 (1996).
[36] G. Rau, A. R. Glanfield, P. C. Klipstein, N. F. Johnson, and G. W. Smith, Phys. Rev. B **60**, 1900 (1999).
[37] M. L. Biermann, J. Diaz-Barriga, and W. S. Rabinovich, Appl. Opt. **42**, 3558 (2003).

[38] M. L. Biermann, S. Duran, K. Peterson, A. Gerhardt, J. W. Tomm, A. Bercha, and W. Trzeciakowski, J. Appl. Phys. **96**, 4056 (2004).
[39] H. Zhu, K. Liu, C. Xiong, S. Feng, and C. Guo, Microelectron. Reliab. **55**, 62 (2015).
[40] K. Liu, H. Zhu, S. Feng, L. Shi, Y. Zhang, and C. Guo, Microelectron. Reliab. **55**, 886 (2015).
[41] R. Balili, V. Hartwell, D. Snoke, L. Pfeiffer, and K. West, Science **316**, 1007 (2007).
[42] R. Balili, B. Nelsen, D. W. Snoke, L. Pfeiffer, and K. West, Phys. Rev. B **79**, 075319 (2009).
[43] D. K. Loginov, A. V. Trifonov, and I. V. Ignatiev, Phys. Rev. B **90**, 075306 (2014).
[44] A. Siarkos, E. Runge, and R. Zimmermann, Phys. Rev. B **61**, 10854 (2000).
[45] R. Zallen and W. Paul, Phys. Rev. **155**, 703 (1967).
[46] L. C. Lew Yan Voon and M. Willatzen, The $k \cdot p$ Method (Springer-Verlag, Berlin, 2009), chap. 7.
[47] G. Pikus, V. Maruschak, and A. Titkov, Fiz. Tekh. Poluprovodn. **22**, 185 (1988) [Sov. Phys. Semicond. **22**, 115 (1988)].
[48] X.-L. Qi and S.-C. Zhang, Rev. Mod. Phys. **83**, 1057 (2011).
[49] A. Pashkin and A. Leitenstorfer, Science **345**, 1121 (2014).
[50] M. Zarenia, A. Perali, D. Neilson, and F. M. Peeters, Sci. Rep. **4**, 7319 (2014).
[51] Y. Nozue, M. Itoh, and K. Cho, J. Phys. Soc. Jpn. **50**, 889 (1981).
[52] In Ref. [43], the normalization of dipole moments squared, $d^2_{\mathrm{h,l}}$, and polarization, $4\pi\mathcal{P}^{(\alpha)}$, to crystal volume, Ω, is erroneously omitted.
[53] P. Etchegoin, J. Kircher, M. Cardona, C. Grein, and E. Bustarret, Phys. Rev. B **46**, 15139 (1992).
[54] P. Etchegoin, J. Kircher, M. Cardona, and C. Grein, Phys. Rev. B **45**, 11721 (1992).
[55] J. D. Plumhof, V. Krapek, F. Ding, K. D. Jons, R. Hafenbrak, P. Klenovsky, A. Herklotz, K. Dorr, P. Michler, A. Rastelli, and O. G. Schmidt, Phys. Rev. B **83**, 121302 (2011).
[56] R. Sooryakumar and P. E. Simmonds, Phys. Rev. B **27**, 4978 (1983).
[57] G. E. Stillman, D. M. Larsen, C. M. Wolfe, and R. C. Brandt, Solid State Commun. **9**, 2245 (1971).
[58] Landolt-Börnstein, Band 17a, Halbleiter (Springer, Berlin, Heidelberg, 1982).
[59] F. Cerdeira, C. J. Buchenauer, F. H. Pollak, and M. Cordona, Phys. Rev. B **5**, 580 (1972).
[60] E. L. Ivchenko and G. E. Pikus, Superlattices and Other Microstructures (Springer-Verlag, Berlin, 1995).
[61] E. V. Ubyivovk, D. K. Loginov, I. Ya. Gerlovin, Yu. K. Dolgikh, Yu. P. Efimov, S. A. Eliseev, V. V. Petrov, O. F. Vyvenko, A. A. Sitnikova, and D. A. Kirilenko, Fiz. Tverd. Tela **51**, 1818 (2009) [Phys. Solid State **51**, 1929 (2009)].
[62] D. Schiumarini, N. Tomassini, L. Pilozzi, and A. D'Andrea, Phys. Rev. B **82**, 075303 (2010).
[63] M. Cardona, Phys. Status Solidi B **198**, 5 (1996).

